

CrossMark
click for updatesCite this: *RSC Adv.*, 2015, 5, 82310

Preparation of amidoxime surface-functionalized polyindole (ASFPI) nanofibers for Pb(II) and Cd(II) adsorption from aqueous solutions

Cai Zhijiang,^{*ab} Jia Jianru,^a Zhang Qing^a and Yang Haizheng^a

Amidoxime surface-functionalized polyindole (ASFPI) nanofibers were prepared by electrospinning of chemically synthesized poly(5-cyanoindole) followed by surface modification. The as-prepared ASFPI nanofibers were characterized with FTIR, SEM, BET surface areas and water contact angle measurement. Meanwhile, the adsorption properties and mechanism of ASFPI nanofibers towards Pb(II) and Cd(II) in aqueous solution were mainly investigated by a batch method. It was found that ASFPI nanofibers showed a high affinity towards Pb(II) and Cd(II). The maximum adsorption capacities were found to be 307.44 and 108.49 mg g⁻¹ for Pb(II) and Cd(II), which are markedly high values compared to other fiber adsorbents reported. The adsorption isotherms were better fitted with the Langmuir model rather than Freundlich and Temkin models. The kinetics data analysis showed that the adsorption process could be described by a pseudo-second order kinetic model, suggesting a chemisorption process as the rate limiting step. Thermodynamic parameters revealed the spontaneity of the adsorption process and higher temperature favored adsorption. Regeneration tests showed that ASFPI nanofibers could be reused repetitively for 10 times with 80% of the initial adsorption capacity.

Received 7th July 2015
Accepted 23rd September 2015

DOI: 10.1039/c5ra13253c

www.rsc.org/advances

1. Introduction

Water pollution by toxic heavy metals has become more and more serious with the rapid increase in global industrial activities. Various methods have been developed for the heavy metals removal such as solvent extraction, membrane separation, precipitation, reduction, electrochemical treatment, adsorption, flocculation, reverse osmosis and ion exchange.¹⁻⁴ Among these methods, adsorption is generally preferred due to its high efficiency, ease of handling and availability of different sorbents.

Nowadays, except various solid adsorbents such as activated carbon, oxide minerals, polymer materials, resins and bio-sorbents,⁵⁻⁸ conducting polymers have been proposed to be used for water treatment. They have shown good prospect for removing heavy metals from aqueous solution due to the presence of nitrogen atoms which can chelate metal ions through electrostatic.⁹ For example, Olad and Kumar^{10,11} have investigated the reduction of toxic Cr(VI) (62.9 mg g⁻¹) in aqueous solution using polyaniline as adsorbent. Ai¹² has prepared polyaniline nanosticks by ultrasonic-assisted method with Cu(II) uptake performance of 7.6 mg g⁻¹. Seid¹³ has

reported the removal of Cd(II) (71.4 mg g⁻¹) and Co(II) (70.04 mg g⁻¹) from aqueous solutions by polypyrrole particles. However, the adsorption capacities of these conducting polymer adsorbents are rather low. It is desirable to develop conducting polymer based adsorbents with higher removal capacity for practical application.

To approach this object, two methods can be adopted. One is to fabricate nano-sized fiber adsorbents with large surface areas and highly active surface sites by nanotechnology. Recently, polyaniline nanofibers and polyacrylonitrile/polypyrrole core/shell nanofibers have been prepared as nano-adsorbents for the removal of Cr(VI) from aqueous solution.^{14,15} Polypyrrole-coated electrospun nanofiber membranes have been reported for recovery of Au(III) from aqueous solution.¹⁶ Polyaniline nanofibers assembled on alginate microsphere have been investigated for Cu(II) and Pb(II) uptake.¹⁷ Another method is to chemically bond the chelating functional groups such as amino, carboxyl, sulfhydryl and amidoxime onto the adsorbents surface.¹⁸⁻²⁰ Among these chelating groups, amidoxime group has a strong chelating ability towards a wide range of heavy metal ions such as UO₂(II), Cu(II), Pd(II), Cd(II).²¹⁻²⁴ Therefore, it would be interesting to investigate the possibility of conducting polymer nanofibers with amidoxime surface functionalization for metal ions adsorption.

Polyindole is a conducting polymer, which possess the properties of both poly(*para*-phenylene) and polypyrrole together, such as fairly good thermal stability, high-redox activity, slow degradation rate in comparison with polyaniline

^aSchool of Textiles, Tianjin Polytechnic University, No. 399 BingShuiXi Street, XiQing District, Tianjin 300387, China. E-mail: caizhijiang@hotmail.com

^bState Key Laboratory of Hollow Fiber Membrane Materials and Processes, No. 399 BingShuiXi Street, XiQing District, Tianjin, 300387, China. Fax: +86-22-83955187; Tel: +86-22-83955385

and polypyrrole, and an air stable electrical conductivity.^{25–28} In this study, amidoxime surface-functionalized polyindole (ASFPI) nanofibers were prepared by electrospinning of poly(5-cyanoindole) followed by surface modification. The ASFPI nanofibers were subsequently used for adsorption of Pd(II) and Cd(II) from aqueous solutions. The factors affecting adsorption properties such as pH value, metal ions concentration, contact time and temperature were investigated using batch method. The equilibrium data were analyzed using Langmuir, Freundlich and Temkin models. Kinetic and thermodynamic parameters of heavy metal ions adsorption were also calculated.

2. Experimental

2.1 Chemicals

5-Cyanoindole, ammonium peroxydisulfate, hydroxylamine hydrochloride, sodium carbonate were purchased from Fluka Chemical Co., LTD and used as received. All other chemicals employed were of analytical reagent grade. Distilled water was used for all preparation and washing stages.

2.2 Preparation of poly(5-cyanoindole)

Poly(5-cyanoindole) was synthesized by suspension polymerization of 5-cyanoindole. 100 mL of chloroform were introduced into a 250 mL round-bottom flask, which was kept at 20 °C under nitrogen. 20 g of ammonium peroxydisulfate were then filled with 10 mL of water. 20 mL of chloroform and 3.2 g of 5-cyanoindole, using the reservoir with a tap, were then introduced in parallel into the flask in the course of 30 minutes. The molar ratio of ammonium peroxydisulfate to 5-cyanoindole was 4. The flask was then kept at 5 °C for 5 hours with stirring. The obtained product was filtered and washed with water and then dried under vacuum.

2.3 Electrospinning of poly(5-cyanoindole)

3 wt% solution was prepared by dissolving poly(5-cyanoindole) in acetonitrile under ultrasonication. The solution was then filled into a glass syringe terminated by a stainless steel needle with inner diameter of 0.40 mm. The syringe was placed in an automatic pump and solution was extruded out at a constant speed of 0.5 mL h^{−1}. A voltage of 25 kV was applied to the needle and the distance between the needle tip and collector was 20 cm. The electrospinning was done in an environmental chamber with constant temperature at 25 °C and relative humidity of 35%.

2.4 Amidoxime surface-functionalization of polyindole (ASFPI) nanofibers

50 mL of 1.0 mol L^{−1} aqueous hydroxylamine hydrochloride solution and 50 mL of 1.0 mol L^{−1} aqueous sodium carbonate solution were mixed (pH = 6.5). The mixed solution was added into a 250 mL beaker, followed by adding 0.5 g of electrospun poly(5-cyanoindole) (EPCI) nanofibers. The amidoximation transform reactions were carried out under N₂ atmosphere at 70 °C for 40 min. The cyano groups (−C≡N) on the surface of EPCI nanofibers reacted with hydroxylamine, leading to the

formation of −C(NH₂)=N−OH groups. After reaction, the obtained ASFPI nanofibers were thoroughly rinsed with water to remove the remaining salts, and dried at 50 °C under vacuum.

2.5 Characterization

The FTIR spectra were recorded using a Perkin Elmer Spectrum RX-I spectrophotometer with the KBr pellet technique. The ¹H NMR spectrum was recorded on a JEOL GAM-ECP600 NMR spectrometer and CDCl₃ was used as the solvent. The surface morphology was observed by scanning electron microscope (SEM, Model TM-3030). BET surface areas were measured by an automatic physisorption analyzer (Micromeritics Instruments). Water contact angle measurement was performed at 25 °C by pendant drop method, employing a contact-angle measurement apparatus (type DSA-10, made in KURSS Company, Germany).

2.6 Adsorption kinetics and equilibrium isotherm of metal ions onto ASFPI nanofibers

Experiments were performed with 0.1 g adsorbent in 250 mL Erlenmeyer flask with 150 mL of single-metal ion solution on a temperature controlled water bath shaker at 300 rpm. All experiments were carried out at 20 °C except the temperature experiments. The metal ions concentration in aqueous phase was determined using a Unicam atomic absorption spectrophotometer (AAS, model 939). The removal efficiency (*R*%) and the quantity of metal ions adsorbed per gram of adsorbent was calculated using eqn (1) and (2).

$$R\% = \left(\frac{C_0 - C_e}{C_0} \right) \times 100 \quad (1)$$

$$q_e = \left(\frac{C_0 - C_e}{m} \right) \times V \quad (2)$$

where *q_e* (mg g^{−1}) is equilibrium sorption capacity, *V* (L) is the volume of metal ions solution, *m* (g) is the weight of dry adsorbent, *C₀* and *C_e* (mg L^{−1}) are the initial and equilibrium concentrations of metal ions, respectively.

The effect of pH on metal ions adsorption was studied by varying the pH value from 1.0 to 7.0 using 0.1 mol L^{−1} HCl and NaOH. The effect of metal ions concentration on adsorption was investigated in a concentration ranging from 50 to 600 mg L^{−1}. To investigate the effect of contact time on adsorption process, samples were withdrawn at different time intervals to determine the ions concentration and the equilibrium time. The isotherm studies were conducted at 20, 30, and 40 °C by varying ions concentration from 100 to 400 mg L^{−1} under the optimum pH.

2.7 Desorption and regeneration experiments

For desorption studies, 0.1 g ASFPI nanofibers mat was first contacted with 200 mL 400 mg L^{−1} Pb(II) and Cd(II) for 12 h at 20 optimum pH and °C, respectively. Then the ASFPI nanofibers mat was rinsed with distilled water to remove any residual solution and was then dried at room condition for 24 h. After that the ASFPI nanofibers mat was immersed into 100 mL 2–10 mol L^{−1} HCl aqueous solutions and shaking at 20 °C for 1 h. The

desorption efficiency (%) was calculated based on the percentage of the ratio between the desorbed and preadsorbed amounts of the ions. Chosen the best eluent determined by desorption efficiency and repeated above processes for ten times to estimate the regeneration performance.

3. Results and discussion

3.1 Preparation of ASFPI nanofibers

In this work, ASFPI nanofibers were prepared from 5-cyanoindole through subsequent steps as presented in Scheme 1. Firstly, poly(5-cyanoindole) was synthesized by suspension polymerization using ammonium peroxydisulfate as oxidants. Poly(5-cyanoindole) nanofibers were then fabricated *via* electrospinning technique. Finally, by the reaction with hydroxylamine which was liberated from neutralization of hydroxylamine hydrochloride and sodium carbonate, the cyano groups on the surface of poly(5-cyanoindole) nanofibers were gradually converted into amidoxime groups ($-\text{C}(\text{NH}_2)=\text{N}-\text{OH}$), forming ASFPI nanofibers. The conversion of cyano groups ($C\%$) and the content of the amidoxime groups (AO) can be determined by eqn (3) and (4).

$$C\% = \left(\frac{W_1 - W_0}{W_0} \right) \times \left(\frac{M_1}{M_0} \right) \times 100 \quad (3)$$

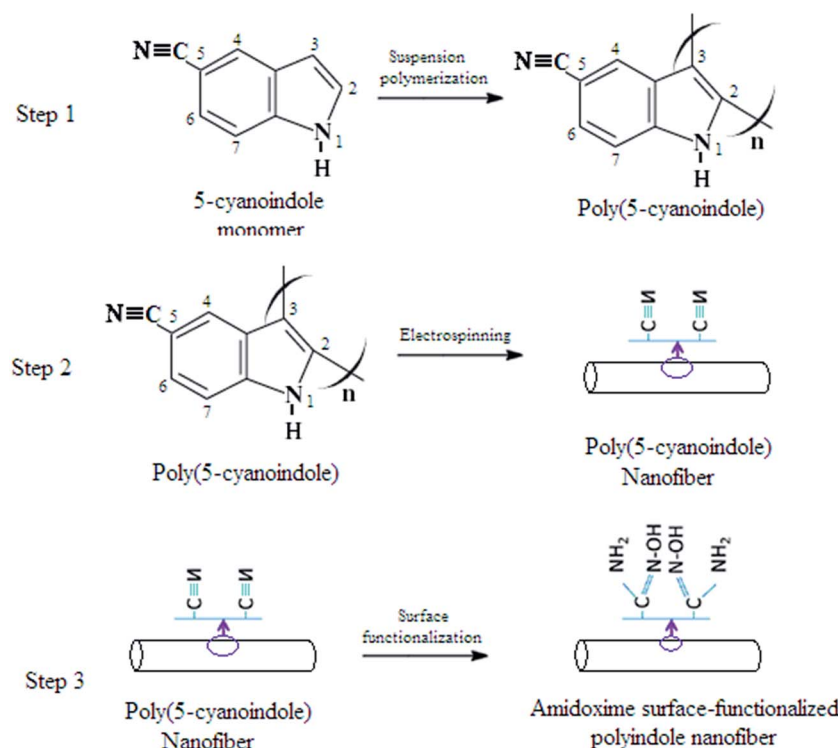
$$\text{AO (mmol g}^{-1}\text{)} = \left(\frac{W_1 - W_0}{W_0} \right) \times \frac{1000}{M_0} \quad (4)$$

where W_0 and W_1 (g) denote the weights of the nanofibers before and after reaction, respectively. M_0 and M_1 (g mol^{-1}) are the

molecular weight of hydroxylamine (33) and 5-cyanoindole (142). The conversion of cyano groups is about 21% and the content of AO on ASFPI nanofibers is about 1.5 mmol g^{-1} accordingly.

3.2 FT-IR study

Fig. 1 shows the FTIR spectra of 5-cyanoindole monomer (a), poly(5-cyanoindole) (b), EPCI nanofibers (c) and ASFPI nanofibers (d). It is observed that the strong and broad band located around 3380 cm^{-1} characteristic to the N-H stretching vibrations occurs in curve (a) and (b). The band at 1504 cm^{-1} in curve (a) and (b) is assigned to the N-H deformations and also the vibration modes of $\text{C}2=\text{C}3$ aromatic bonds, typical of indole. These results imply the presence of N-H bonds on poly(5-cyanoindole) backbone. Thus, nitrogen atom is likely not the polymerization site. A sharp band around 2215 cm^{-1} can be observed in curve (a) and (b), which corresponds to the characteristic stretching vibrations of cyano group. A sharp peak at 741 cm^{-1} and the band at 1455 cm^{-1} observed in curve (a) and (b) are attributed to the characteristic out of plane deformations of the C-H bond in the benzene ring and stretching of benzene ring, respectively. These results suggest that the benzene ring is also not involved in the polymerization. A peak around 720 cm^{-1} in curve (a) is assigned to the characteristic feature of the in-phase vibrations of hydrogen species ascribed to the C2 and C3 of 5-cyanoindole monomer. However, this band is found to be absent in curve (b). This result indicates that C2 and C3 of indole ring should be the possible sites of polymerization.



Scheme 1 Schematic illustration of preparation process of ASFPI nanofibers.

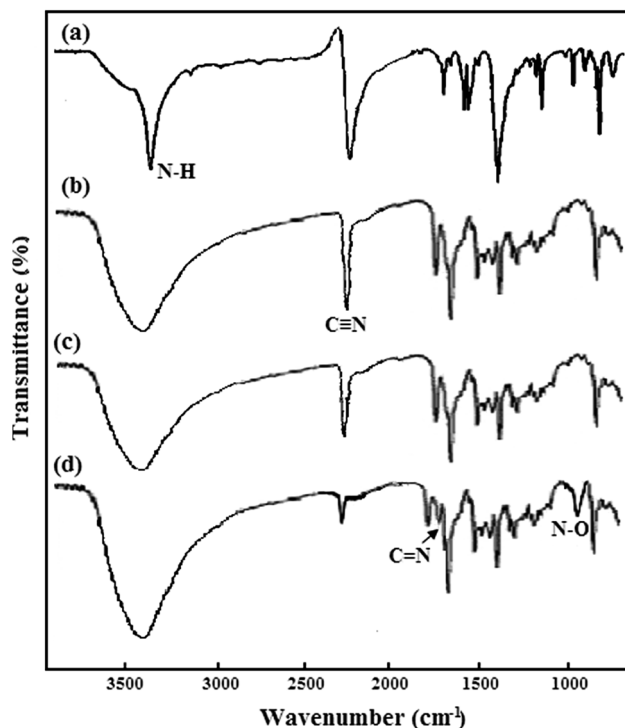


Fig. 1 FTIR spectra of 5-cyanoindole monomer (a), poly(5-cyanoindole) (b), EPCI nanofibers (c) and ASFPI nanofibers (d).

The spectra of EPCI nanofibers are same to poly(5-cyanoindole), which confirms the structural stability of poly(5-cyanoindole) during the electrospinning process. After amidoximation, the band of cyano group ($\text{C}\equiv\text{N}$) at 2215 cm^{-1} almost disappears. There appear two new bands at 1640 cm^{-1} and 950 cm^{-1} . The former should be ascribed to the vibrations absorption of $\text{C}=\text{N}$ bond in amidoxime group, and the latter should be attributed to the vibrations absorption of $\text{N}-\text{O}$ bond in amidoxime group. From the FTIR spectra, the introduction of amidoxime groups on polyindole nanofibers can be confirmed.

3.3 ^1H NMR test

To further confirmation of the amidoxime groups on polyindole nanofibers, the ^1H NMR spectra of EPCI and ASFPI nanofibers were recorded and shown in Fig. 2. In the spectrum of EPCI

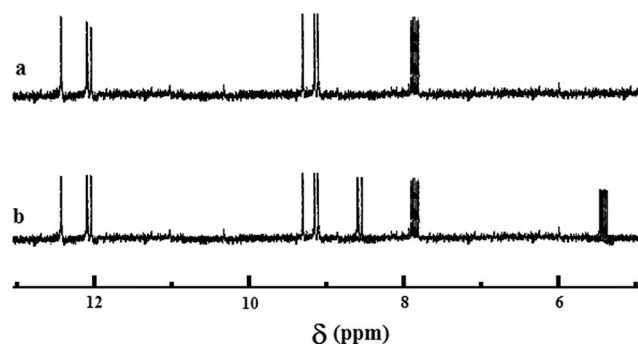


Fig. 2 ^1H NMR spectra of the EPCI (a) and ASFPI (b) nanofibers.

nanofibers, there are three groups of proton peaks. The peaks at 12.01, 12.07 and 12.58 ppm represent proton of $\text{N}-\text{H}$. The other three peaks between 9.1 and 9.4 ppm arise from the proton at 4-position of the benzene ring. Multiple of peaks attributed to the protons at 6 and 7-positions of benzene ring appear in region 7.8–7.9 ppm. All peaks in the ^1H NMR spectrum of EPCI are in agreement with the spectrum of poly(5-cyanoindole).²⁹ In the ^1H NMR spectrum of ASFPI nanofibers, two new groups of proton peaks can be detected. The peaks appearing around 5.4 ppm and 8.7 ppm are assigned to $-\text{NH}_2$ and $-\text{OH}$ protons. Comparison of the ^1H NMR spectrum of EPCI nanofibers with ASFPI nanofibers clearly proves that $\text{C}\equiv\text{N}$ groups on the EPCI converted successfully to amidoxime groups ($-\text{C}(\text{NH}_2)=\text{N}-\text{OH}$).

3.4 Characteristic of nanofibers

The SEM images and fiber diameter distributions of EPCI and ASFPI nanofibers are presented in Fig. 3. EPCI nanofibers exhibit smooth surface, round shape and are randomly oriented. The average diameter and BET surface areas are about $234 \pm 35\text{ nm}$ and $61.71\text{ m}^2\text{ g}^{-1}$, respectively. After amidoximation, the as-prepared ASFPI nanofibers become densely packed and the average diameter slightly increases to $252 \pm 42\text{ nm}$. The reason might be attributed to the surface amidoxime groups, which can absorb water in air. No degradation or cracks appear on ASFPI nanofibers, which show almost same morphology to EPCI nanofibers.

The average diameter, BET surface areas and water contact angle of EPCI and ASFPI nanofibers are collected in Table 1. It is noteworthy that poly(5-cyanoindole) is hydrophobic while amidoxime is much more hydrophilic. Amidoximation of EPCI nanofibers result in the formation of $-\text{C}(\text{NH}_2)=\text{N}-\text{OH}$ groups on the fibers surface, leading to considerable increase of hydrophilicity. The high hydrophilicity as well as large BET surface areas of ASFPI nanofibers favors metal ions uptake.

3.5 Adsorption behaviors

3.5.1 Effect of amidoximation on removal of metal ions.

Surface functionalization can significantly improve the adsorption capacities of adsorbents. The effect of amidoxime surface-functionalization on metal ions removal was investigated using EPCI and ASFPI nanofibers as adsorbent and the results are given in Fig. 4. It is observed that the removal efficiency increases with an increase in adsorbent dose. This is due to an increase in the surface areas and availability of more active sites for sorption. The amounts of EPCI nanofibers required for the complete removal of $\text{Pb}(\text{II})$ and $\text{Cd}(\text{II})$ from their solutions are 70 and 120 mg, respectively. However, the amounts of ASFPI nanofibers required for the complete removal of $\text{Pb}(\text{II})$ and $\text{Cd}(\text{II})$ are 40 and 60 mg respectively. The adsorption capacity of the ASFPI nanofibers is therefore about 1.75–2.0 times (1.75 for $\text{Pb}(\text{II})$, 2.0 for $\text{Cd}(\text{II})$) higher than that of EPCI nanofibers. The significant increase in metal ions adsorption capacity is attributed to the presence of amidoxime groups on ASFPI nanofibers. This result clearly indicates that amidoxime surface-functionalization can greatly improve the adsorption efficiency of polyindole nanofibers for metal ions.

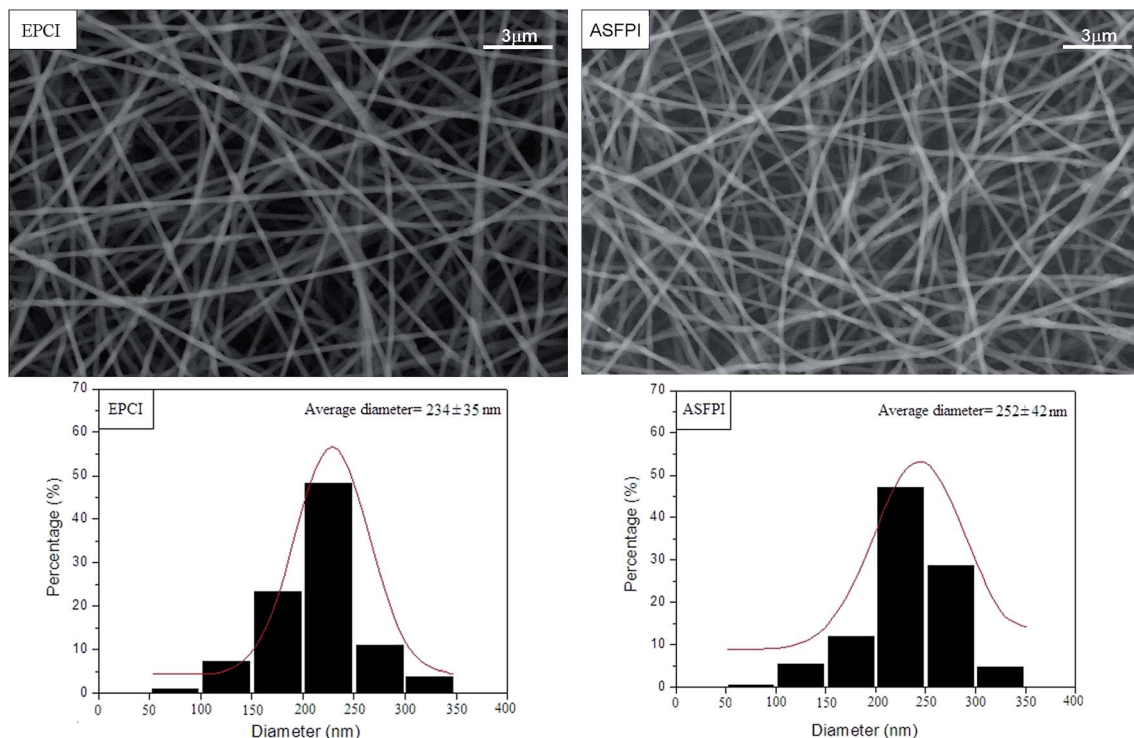


Fig. 3 SEM images and fiber diameter distribution of EPCI and ASFPI nanofibers.

Table 1 The characteristics of EPCI and ASFPI nanofibers

Nanofibers	Average diameter (nm)	BET surface areas ($\text{m}^2 \text{g}^{-1}$)	Water contact angle ($^\circ$)
EPCI	234 ± 35	61.71	124
ASFPI	252 ± 42	59.36	76

3.5.2 Effect of pH and adsorption mechanism. Acidity is one of the key parameters in metal ions adsorption from aqueous solution. It not only affects the speciation of metal ions but also influences the ionization of functional groups on the surface of adsorbent. Fig. 5 presents the effect of solution pH on Pb(II) and Cd(II) adsorption by ASFPI nanofibers. It can be observed that the Pb(II) and Cd(II) adsorption by ASFPI nanofibers is pH dependent. As $\text{pH} < 5$, the adsorption capacities increase with increasing pH value; as $\text{pH} = 5$, maximum adsorption capacities of 216.64 and 66.27 mg g^{-1} for Pb(II) and Cd(II) are achieved; as $\text{pH} > 5$, the adsorption capacities turn to decline with pH value increasing. The reason can be explained as following. At low pH, the nitrogen atom and amino groups of amidoxime on the surface of ASFPI nanofibers will lose the complex ability towards metal ions due to high protonation (seen eqn (5)), leading to low adsorption capacity. With pH value increasing the degree of protonation of the nitrogen atom and amino groups gradually reduce. In addition, the dissociation degree of oxime-hydroxyl-groups increases and negative oxygen-ion of oxime-hydroxyl-groups can be produced (seen eqn (6)), which result in gradual increasement in adsorption

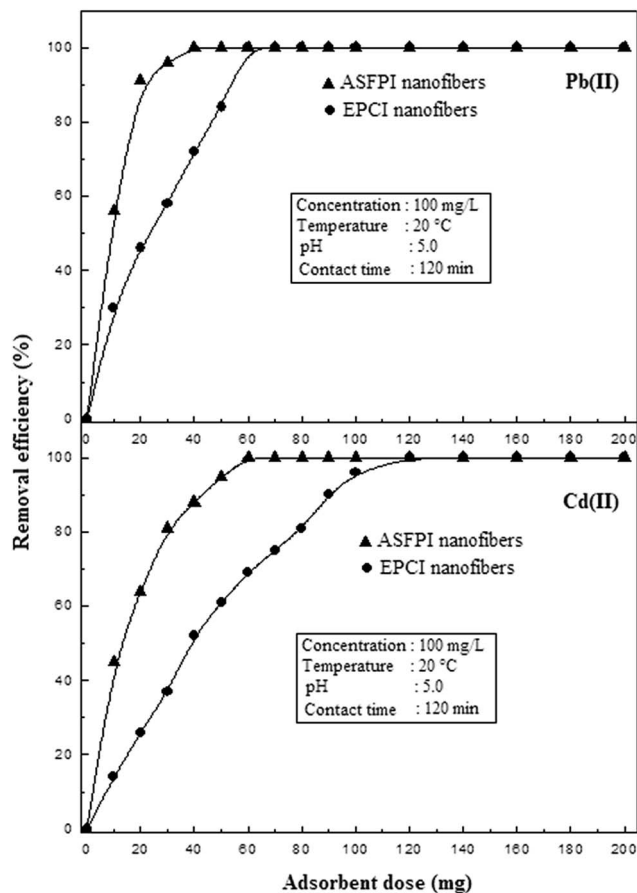


Fig. 4 Effect of adsorbent dose on the removal efficiency of Pb(II) and Cd(II) by EPCI and ASFPI nanofibers.

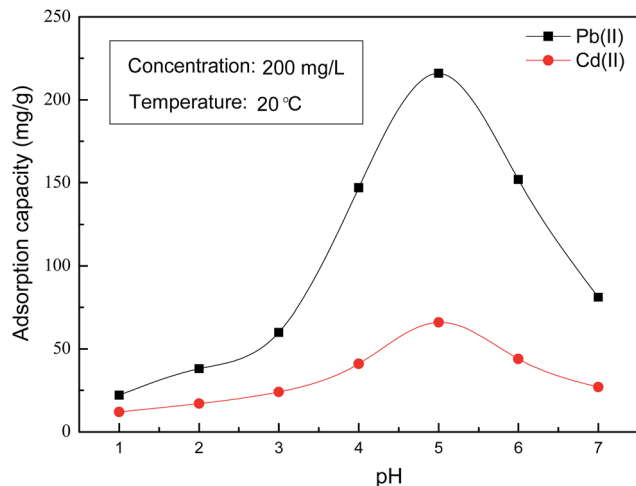
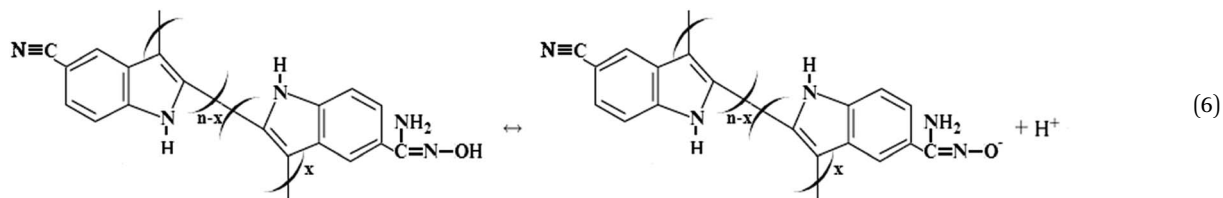
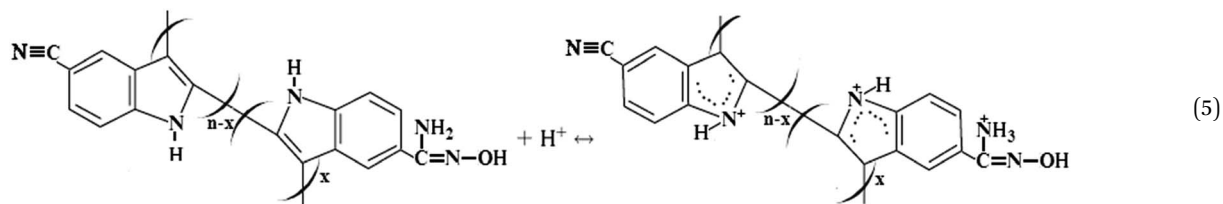


Fig. 5 The effect of solution pH on Pb(II) and Cd(II) adsorption by ASFPI nanofibers.

capacity.²² As $\text{pH} > 5$, the hydrolysis of metal ions becomes obvious which leads to the decline of the adsorption ability. Thus, all the following experiments are therefore performed at pH 5.

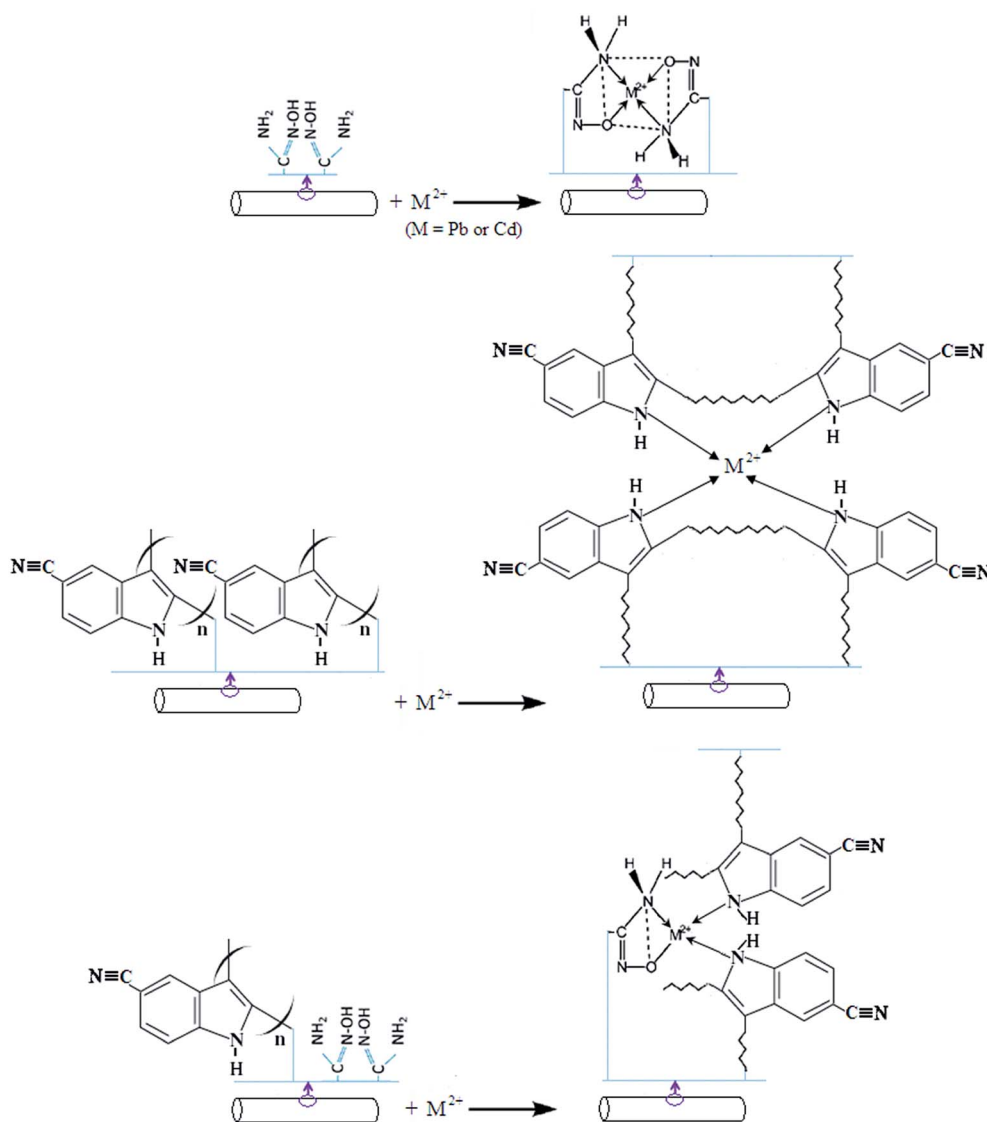
The adsorption capacity of ASFPI nanofibers for Pb(II) is much higher than Cd(II). The explanation for preferential sorption behavior is based on two facts. The first is that the hydrated ionic radius of Cd(II) is much bigger than that of Pb(II). The smaller metal ion (Pb(II)) has the higher adsorption capacity, which may be attributed to the fact that the smaller particles could reach easily to the active adsorption sites. We believe that there are some sterical hindrances, and therefore, ionic radii of the metal ions are playing important role in determining the adsorption capacity. The second reason is due to the relative stability of the complexes formed by Pb(II) and Cd(II) with amidoxime group. According to the Irving–Williams concept based on ligand field,³⁰ the stability of metal cation-oxygen donor complexes decreases in the series: $\text{Pb(II)} > \text{Cd(II)}$. The observed order of uptake for metal ions is the same as that of their increasing metals first hydrolysis constant. The logarithmic values of the metals first hydrolysis constant of the metal ions studied are as follows: $\log K_{\text{Pb}} = -7.71$, $\log K_{\text{Cd}} = -10.08$.³¹ Metal ions which form less soluble hydroxides are adsorbed more easily.

3.5.3 Effect of initial concentration and adsorption isotherm. Fig. 6 shows the effect of initial metal ions concentration on equilibrium adsorption of ASFPI nanofibers. It is



The adsorption action of ASFPI nanofibers for Pb(II) and Cd(II) should be a chemical sorption involving valence forces through sharing or exchange of electrons between adsorbent and adsorbate. The chelation of Pb(II) and Cd(II) onto ASFPI nanofibers can be explained with coordination between the electron-donating nature of O^- and N-containing groups on the surface of the fibers and electron-accepting nature of metal ions. Owing to the presence of two chelating components in ASFPI nanofibers, there are various possibilities for binding metal ions on the adsorbent. Scheme 2 presents possible adsorption mechanism of chelation of metal ions: chelation by the amidoxime groups (reaction I), chelation on the polyindole chains by the nitrogen atoms (reaction II), and chelation by the cooperation of amidoxime groups and nitrogen atoms of polyindole chains (reaction III).

clear that the amount of metal ions adsorbed onto ASFPI nanofibers is increased with ions concentration increasing, and then reaches a plateau value. The equilibrium adsorption capacities increase from 65.26 to 307.44 mg g^{-1} for Pb(II) and 36.41 to 108.49 mg g^{-1} for Cd(II) when initial ions concentration increases from 50 to 600 mg L^{-1} . In the case of low concentrations ($<400 \text{ mg L}^{-1}$ for Pb, 300 mg L^{-1} for Cd), the ratio of the available adsorption sites to the initial number of metal ions is larger and, subsequently, the fractional ion exchange becomes independent of initial concentrations. If the concentration is high ($>400 \text{ mg L}^{-1}$ for Pb, 300 mg L^{-1} for Cd), ASFPI nanofibers could only achieve the saturation adsorption. This result shows that the removal of Pb(II) and Cd(II) by ASFPI nanofibers is highly concentration-dependent.



Scheme 2 Possible adsorption mechanisms of ASFPI nanofibers for Pb(II) and Cd(II).

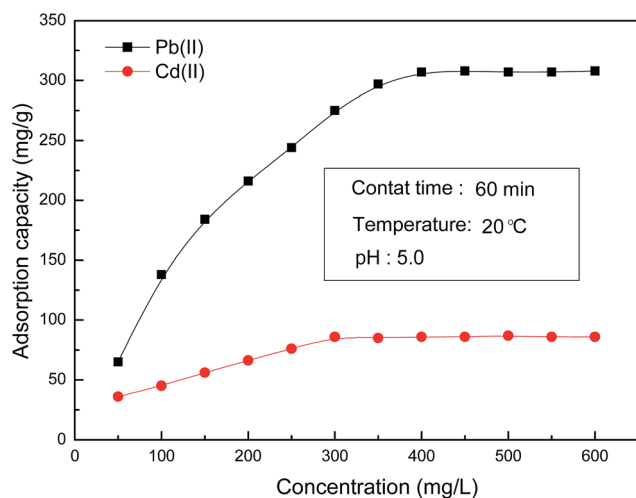


Fig. 6 The effect of initial ions concentration on Pb(II) and Cd(II) adsorption by ASFPI nanofibers.

The adsorption isotherm of ASFPI nanofibers is investigated by Langmuir, Freundlich and Temkin models, respectively. The Langmuir model assumes that the uptake of metal ions occurs on a homogeneous surface by monolayer adsorption without any interaction between adsorbed ions. The Freundlich model assumes that the adsorption of metal ions occurs on a heterogeneous surface by monolayer adsorption. The Temkin model assumes that the heat of adsorption of the molecules decreases linearly due to sorbent-sorbate interactions. The Langmuir, Freundlich and Temkin model can be represented in the linearized form as:

$$\frac{C_e}{q_e} = \frac{1}{Q_m \times K_L} + \frac{C_e}{Q_m} \quad (7)$$

$$\ln q_e = \ln K_F + \frac{\ln C_e}{n} \quad (8)$$

$$q_e = \frac{RT}{B_T} \ln K_T + \frac{RT}{B_T} \ln C_e \quad (9)$$

where Q_m (mg g^{-1}) is the maximum adsorption capacity, K_L (L mg^{-1}) is the Langmuir constant related to the energy of adsorption, K_F (mg g^{-1}) is the Freundlich constant related to the adsorption capacity and n is the heterogeneity factor, K_T (L g^{-1}) is the equilibrium binding constant corresponding to the maximum binding energy, B_T (kJ mol^{-1}) is the Temkin constants related to the heat of adsorption, R ($8.314 \text{ J mol}^{-1} \text{ K}^{-1}$) is the universal gas constant and T (K) is the absolute temperature.

The Langmuir, Freundlich and Temkin isotherm parameters for Pb(II) and Cd(II) adsorption by ASFPI nanofibers can be determined from the intercept and slope of the linear fitting line by plotting C_e vs. C_e/q_e (Fig. 7A), $\ln q_e$ vs. $\ln C_e$ (Fig. 7B) and q_e vs. $\ln C_e$ (Fig. 7C). The obtained parameter values as well as

the correlation coefficient (R^2) are summarized in Table 2. Comparison of R^2 values indicate that adsorption of Pb(II) and Cd(II) by ASFPI nanofibers is described better by Langmuir model ($R^2 = 0.998$ for Pb(II), 0.990 for Cd(II)) than Freundlich and Temkin models ($R^2 = 0.833$ for Pb(II), 0.924 for Cd(II) and $R^2 = 0.943$ for Pb(II), 0.915 for Cd(II)) at the studied temperature. The Q_m calculated by Langmuir model is 327.87 and 98.62 mg g^{-1} for Pb(II) and Cd(II), consistent with the actual saturated adsorption capacity (Pb(II) 307.44 mg g^{-1} , Cd(II) 108.49 mg g^{-1}) of ASFPI nanofibers, which also proves the monolayer adsorption is dominated.

Moreover, using Langmuir parameters, the dimensionless separation factor R_L could be calculated using eqn (10).

$$R_L = \frac{1}{1 + K_L C_0} \quad (10)$$

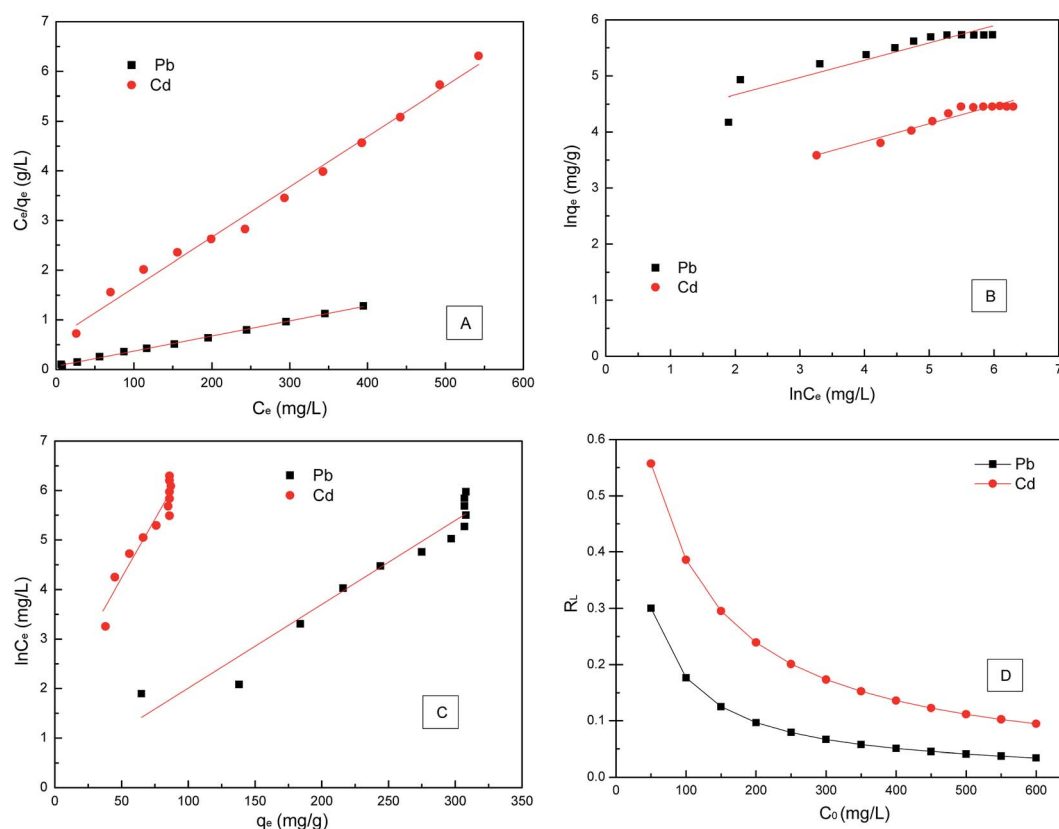


Fig. 7 Sorption isotherm displayed in their linearized format and fit by the Langmuir model (A), Freundlich model (B) and Temkin model (C) and the variation of R_L with initial concentration of metal ions (D).

Table 2 Langmuir, Freundlich and Temkin isotherm parameters for Pb(II) and Cd(II) adsorption by ASFPI nanofibers

Metal ions	Langmuir model			Freundlich model			Temkin model		
	Q_m (mg g^{-1})	K_L (L mg^{-1})	R^2	K_F (mg g^{-1})	n	R^2	K_T (L g^{-1})	B_T (kJ mol^{-1})	R^2
Pb	327.87	0.0466	0.998	56.98	3.24	0.833	120.25	0.143	0.943
Cd	98.62	0.0159	0.990	12.77	3.12	0.924	539.47	0.0513	0.915

The variation of R_L with initial metal ions concentration is plotted in Fig. 7D. This factor can suggest the favorability of an adsorption process. R_L represents the adsorption process to be unfavorable ($R_L > 1$), linear ($R_L = 1$), favorable ($0 < R_L < 1$), or irreversible ($R_L = 0$). For all initial concentration studied, R_L values of Pb(II) and Cd(II) fall between 0 and 1, confirming the favorable nature of adsorption by the ASFPI nanofibers. The R_L values decrease with initial concentration increasing, as shown in Fig. 7D. This result indicates that Pb(II) and Cd(II) adsorption is more favorable at higher initial concentration.³²

A comparison of the as-prepared ASFPI nanofibers with those of some other fiber adsorbents for the adsorption of Pb(II) and Cd(II) in recently reported literature is summarized in Table 3. As shown in Table 3, the maximum adsorption capacity of Pb(II) and Cd(II) by ASFPI nanofibers is comparable with that of other effective fiber adsorbents, and therefore ASFPI nanofibers could be recommended as an efficient alternative for the sorption of Pb(II) and Cd(II) from aqueous solution.

3.5.4 Effect of contacting time and adsorption kinetics.

Fig. 8 displays the effect of contact time on the adsorption of metal ions by ASFPI nanofibers. It is evident that adsorption rate is fast in the initial stage of the process, then slows down markedly, and gradually reaches plateau. Equilibrium is attained within 30 and 45 min for Pb(II) and Cd(II), respectively. The half-load time ($t^{1/2}$) is less than 5 min for both metal ions. The high initial rate implies that the adsorption occurs essentially on the surface of ASFPI nanofibers. The adsorption rate of Pb(II) is higher than Cd(II) which might be due to higher affinity of the interacting amidoxime groups on the surface of ASFPI nanofibers.

In order to better understand the adsorption kinetic of Pb(II) and Cd(II) sorption onto ASFPI nanofibers, two commonly used kinetic models, namely, the Lagergren's pseudo-first-order and pseudo-second-order model are used. The pseudo-first-order

model assumes diffusion is the rate limiting step of the adsorption process. On the hand, pseudo-second-order model assumes chemisorption as the rate limiting step. The pseudo-first-order and the pseudo-second-order equations can be linearly expressed as follows:

$$\log(q_e - q_t) = \log q_e - \left(\frac{K_1}{2.303}\right)t \quad (11)$$

$$\frac{t}{q_t} = \frac{1}{K_2 q_e^2} + \left(\frac{1}{q_e}\right)t \quad (12)$$

where q_t (mg g^{-1}) is the adsorption capacity at time t (min), K_1 (min^{-1}) is the pseudo-first-order rate constant, and K_2 ($\text{g mg}^{-1} \text{min}^{-1}$) is the pseudo-second-order rate constant. The kinetic parameters for pseudo-first-order and pseudo-second-order

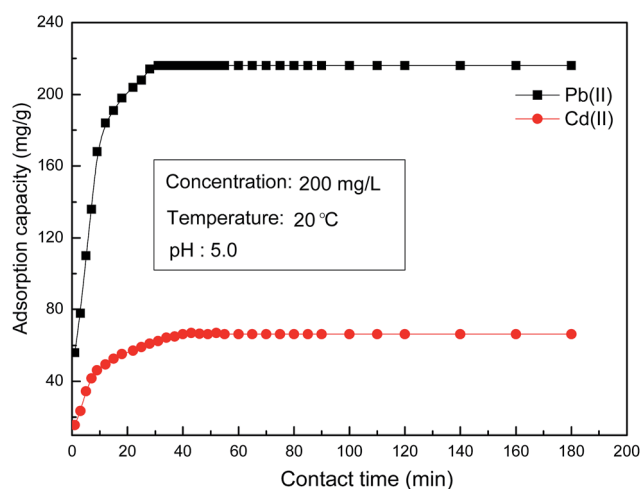


Fig. 8 The effect of contact time on Pb(II) and Cd(II) adsorption by ASFPI nanofibers.

Table 3 Comparison of the adsorption capacity of ASFPI nanofibers with those of some other fiber adsorbents reported in literature for the adsorption of Pb(II) and Cd(II)

Adsorbents	Metal ions	Operating conditions	Adsorption capacity	Ref.
Chitosan coated cotton fiber	Pb(II)	1 mmol L ⁻¹ pH 6.5	101.65 mg g ⁻¹	33
	Cd(II)		15.76 mg g ⁻¹	
Diethylenetriamine pentaacetic acid modified kapok fiber	Pb(II)	400 mg L ⁻¹ pH 5.5	310.6 mg g ⁻¹	34
	Cd(II)		163.7 mg g ⁻¹	
Amidoximated polyester fiber	Pb(II)	130 mg L ⁻¹ pH 6	66.84 mg g ⁻¹	35
	Cd(II)		13.11 mg g ⁻¹	
Activated carbon fiber	Pb(II)	100 mg L ⁻¹ pH 5.6	232.4 mg g ⁻¹	36
	Cd(II)		33.8 mg g ⁻¹	
Electrospun cellulose nanofibers modified with oxolane-2,5-dione	Pb(II)	100 mg L ⁻¹ pH 6	250.47 mg g ⁻¹	37
	Cd(II)		66.32 mg g ⁻¹	
Amphiprotic cotton fiber	Pb(II)	400 mg L ⁻¹ pH 6	70.6 mg g ⁻¹	38
Carboxylated bamboo fibers	Pb(II)	100 mg L ⁻¹ pH 5.6	127.1 mg g ⁻¹	39
PAA modified electrospun cellulose acetate nanofiber membranes	Cd(II)	30 mg L ⁻¹ pH 6	3.04 mg g ⁻¹	40
Aminated electrospun polyacrylonitrile nanofiber mats	Pb(II)	40 mg L ⁻¹ pH 4	60.6 mg g ⁻¹	41
Polyaniline nanofibers assembled on calcium alginate microsphere	Pb(II)	10 mg L ⁻¹ pH 7	251.25 mg g ⁻¹	17
Amidoxime surface-functionalized polyindole (ASFPI) nanofibers	Pb(II)	400 mg L ⁻¹ pH 5	307.44 mg g ⁻¹	This study
	Cd(II)		108.49 mg g ⁻¹	

model are calculated from the intercept and slope of the linear fitting line by plotting $\log(q_e - q_t)$ vs. t (Fig. 9a) and (t/q_t) vs. t (Fig. 9b), respectively.

As seen from the results listed in Table 4, the pseudo-second-order model provides better correlation coefficients ($R^2 = 0.995$ for Pb(II) and 0.996 for Cd(II)) than the pseudo-first-order model ($R^2 = 0.868$ for Pb(II) and 0.888 for Cd(II)). Simultaneously, the good agreement between the calculated $q_{e,cal}$ values (299.40 mg g^{-1} for Pb(II), 95.60 mg g^{-1} for Cd(II)) and the experimental $q_{e,exp}$ values (307.44 mg g^{-1} for Pb(II), 108.49 mg g^{-1} for Cd(II)) suggests that the adsorption kinetic closely follows the pseudo-second-order model rather than the pseudo-first-order model. This indicates that the rate-limiting step may be chemisorption

promoted by covalent/valence forces through exchange or sharing of electrons between adsorbent and adsorbate.

Furthermore, intra-particle diffusion model is also used to analyze the rate-limiting step in adsorption. The model can be expressed by the Weber–Morris equation as following:

$$q_t = K_{ip}t^{0.5} + C \quad (13)$$

where K_{ip} ($\text{mg g}^{-1} \text{min}^{-0.5}$) is the intra-particle diffusion rate constant and the intercept C (mg g^{-1}) is constant related to the thickness of boundary layer. It is postulated that the intra-particle diffusion is considered to be the rate limiting step when the plot of q_t vs. $t^{0.5}$ yields a straight line that passes through the origin.

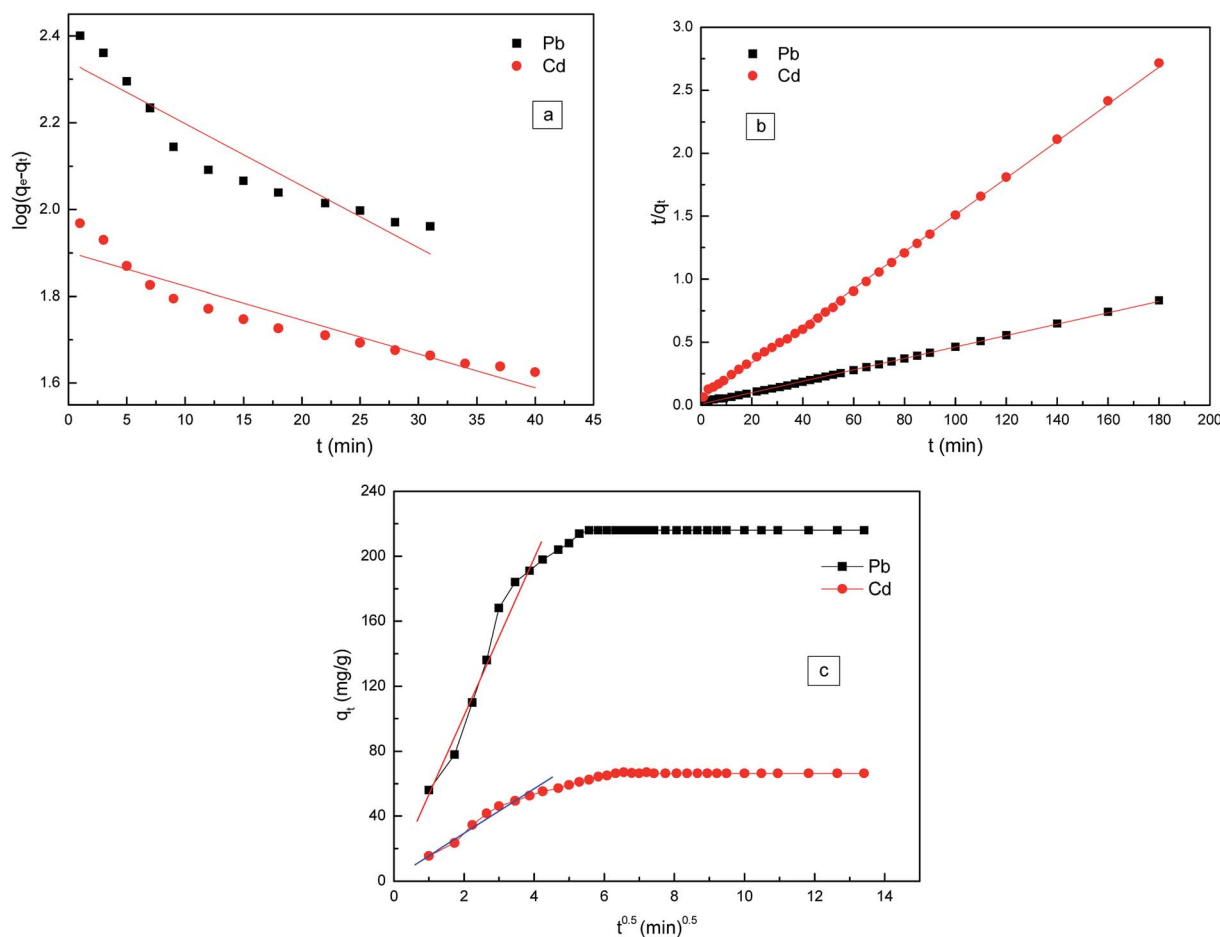


Fig. 9 Data fitting for Pb(II) and Cd(II) adsorption by ASFPI nanofibers using pseudo-first-order kinetic model (a), pseudo-second-order kinetic model (b) and intra-particle diffusion model (c).

Table 4 Kinetic parameters for Pb(II) and Cd(II) adsorption by ASFPI nanofibers

Ions	$q_{e,exp}$ (mg g^{-1})	Pseudo-first-order model			Pseudo-second-order model			Intra-particle diffusion model		
		K_1 (min^{-1})	$q_{e,cal}$ (mg g^{-1})	R^2	K_2 ($\text{g mg}^{-1} \text{min}^{-1}$)	$q_{e,cal}$ (mg g^{-1})	R^2	K_{ip} ($\text{mg g}^{-1} \text{min}^{-0.5}$)	C (mg g^{-1})	R^2
Pb(II)	307.44	0.0952	206.19	0.868	0.000565	299.40	0.995	48.41	5.81	0.958
Cd(II)	108.49	0.180	79.73	0.888	0.00142	95.60	0.996	13.68	2.52	0.965

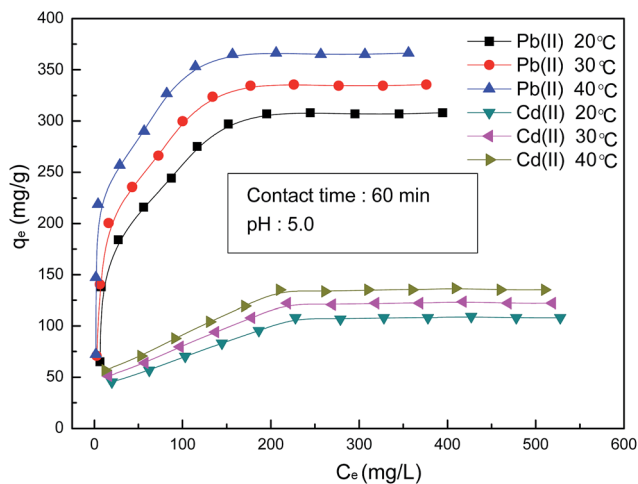


Fig. 10 The effect of temperature on Pb(II) and Cd(II) adsorption by ASFPI nanofibers.

The plot of q_t vs. $t^{0.5}$ is given in Fig. 9c. The adsorption plots of Pb(II) and Cd(II) do not pass through the origin suggesting that intra-particle diffusion is not the only rate limiting step. This behavior indicates that the Pb(II) and Cd(II) adsorption processes by ASFPI nanofibers involve more than one single kinetic stage. The initial rapid adsorption of metal ions may be governed by boundary layer diffusion and the subsequent slow uptake is attributed to the intra-particle diffusion effect.⁴² The values of K_{ip} and C are obtained from the slope and intercept of the linear part of the plot of q_t vs. $t^{0.5}$ (Fig. 9c) and listed in Table 4 along with the correction coefficients. The higher value of K_{ip} for Pb(II) obtained indicates that ASFPI nanofibers exhibit faster removal of Pb(II) from aqueous solutions.

3.5.5 Effect of temperature and adsorption thermodynamics. To investigate the effect of temperature on the adsorption of Pb(II) and Cd(II) by ASFPI nanofibers, adsorption experiments were carried out at three different temperatures (20, 30 and 40 °C) and the results are shown in Fig. 10. It can

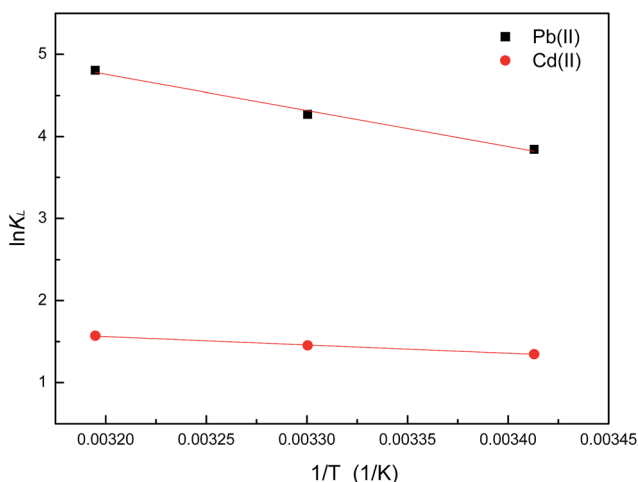


Fig. 11 Plot to determine thermodynamic parameters for Pb(II) and Cd(II) adsorption by ASFPI nanofibers.

Table 5 Thermodynamic parameters for Pb(II) and Cd(II) adsorption by ASFPI nanofibers

Metal ions	ΔG° (kJ mol ⁻¹)			ΔH° (kJ mol ⁻¹)	ΔS° (J mol ⁻¹ K ⁻¹)	R^2
	293 K	303 K	313 K			
Pb(II)	-9.36	-10.40	-11.70	36.53	156.40	0.986
Cd(II)	-6.74	-7.43	-7.71	8.49	40.15	0.994

be seen that the adsorption capacities at equilibrium increase from 307.44 to 365.65 mg g⁻¹ for Pb(II) and 108.49 to 134.58 mg g⁻¹ for Cd(II) with temperature increasing from 20 to 40 °C. As we known that the physical adsorption is an exothermic process, and the adsorption capacity always decreases with raising temperatures. It is apparent that the adsorption of Pb(II) and Cd(II) by ASFPI nanofibers is an endothermic process implying a chemical adsorption process.⁴³ This chemical adsorption is originated from the coordination and chelating action of the nitrogen atoms and amidoxime groups of ASFPI nanofibers towards Pb(II) and Cd(II) as we discussed before.

The thermodynamics parameters of Pb(II) and Cd(II) adsorption by ASFPI nanofibers, such as ΔG° , ΔH° and ΔS° can be evaluated by the van't Hoff equation (eqn (14)), which correlates ΔH° and ΔS° with Langmuir equilibrium constant, K_L .

$$\ln K_L = \frac{\Delta S^\circ}{R} + \frac{-\Delta H^\circ}{RT} \quad (14)$$

The slope, $\Delta H^\circ/R$ and the intercept $\Delta S^\circ/R$ obtained by plotting $\ln K_L$ vs. $1/T$ (Fig. 11) according to eqn (14) give ΔH° and ΔS° values, which are listed in Table 5. On the basis of the values of K_L as a function of temperatures, ΔG° values are calculated by eqn (15) and listed in Table 5.

$$\Delta G^\circ = -RT \ln K_L \quad (15)$$

The positive values of ΔH° indicate that Pb(II) and Cd(II) adsorption by ASFPI nanofibers is an endothermic process. The

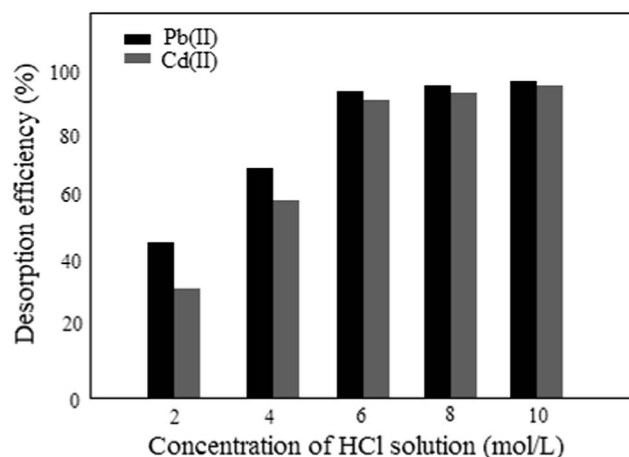


Fig. 12 Desorption of Pb(II) and Cd(II) from the metal-loaded ASFPI nanofibers in HCl solution.

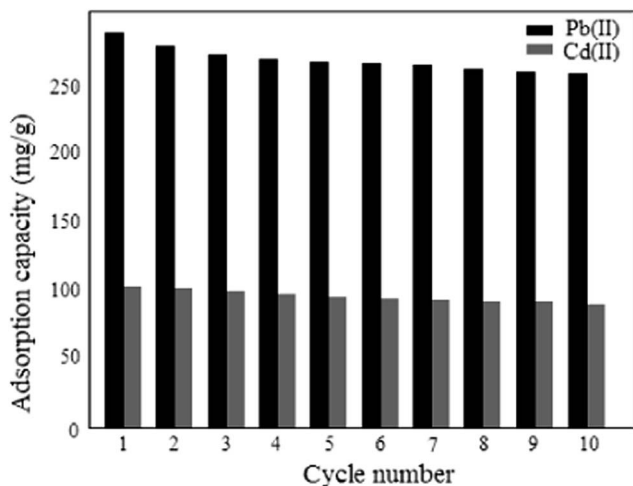


Fig. 13 Adsorption capacities of ASFPI nanofibers after regeneration.

positive values of ΔS° result from the increased randomness at the solid–solution interface due to the adsorption of metal ions. The negative values of ΔG° reveal that the adsorption process is spontaneous and thermodynamically favorable. The increase of the negative values of ΔG° with the increase of temperature suggests an increased trend in the degree of spontaneity of the metal ions sorption. The thermodynamics parameters of ASFPI nanofibers for Pb(II) and Cd(II) adsorption imply chemisorption rather than physisorption, which are fitted to the deduction obtained from the adsorption kinetics.

3.6 Desorption and reusability

For the potential application of ASFPI nanofibers in industrial wastewater treatment, reusability is very important. The desorption behavior of ASFPI nanofibers is graphically shown in Fig. 12. It is found that increasing the HCl concentration results in a monotonous increase in the desorbed amounts of the metal ions. Based on the obtained results, the desorption efficiency of over 90% (93% for Pb(II) and 91% for Cd(II)) could be achieved with the use of 6 mol L⁻¹ HCl solution as the desorbing solution. After desorption, repeated adsorption/desorption cycles are performed to examine the reusability of the ASFPI nanofibers and the results are shown in Fig. 13. It could be found out that the ASFPI nanofibers have good reusability performance. After ten cycles, the adsorption capacities remain 255.18 mg g⁻¹ for Pb(II) and 86.79 mg g⁻¹ for Cd(II), which are about 83% and 80% of the new ASFPI nanofibers.

4. Conclusion

By using a three-step process, suspension polymerization of 5-cyanoindole, electrospinning of poly(5-cyanoindole) and surface-functionalization of EPCI nanofibers, ASFPI nanofibers were successfully prepared. Amidoxime surface-functionalization can greatly improve the metal ions adsorption efficiency. The maximum adsorption capacities of ASFPI nanofibers follow the order Pb(II) > Cd(II). The reason can be explained in terms of the hydrated ionic radius and relative stability of the complexes.

The experimental data fit well with Langmuir isotherm equation and pseudo-second-order kinetic model, which indicate that the chemisorption is the controlling mechanism and the monolayer adsorption is dominated. The adsorption process is spontaneous and endothermic. ASFPI nanofibers could be reused repetitively for 10 times with more than 80% of initial adsorption capacity. These results strongly suggest that ASFPI nanofibers have promising potential as an adsorbent for the removal of heavy metal ions from aqueous solutions and industry wastewaters.

Nomenclature

q_e	Equilibrium sorption capacity (mg g ⁻¹)
q_t	Adsorption capacity at time t (mg g ⁻¹)
V	Solution volume (L)
m	The amount of added adsorbent (g)
M	The molecular weight (g mol ⁻¹)
W	The weight (g)
C_0	Initial Pb(II) concentrations (mg L ⁻¹)
C_e	Equilibrium Pb(II) concentrations (mg L ⁻¹)
Q_m	Maximum adsorption capacity (mg g ⁻¹)
K_L	The Langmuir constant (L mg ⁻¹)
K_F	The Freundlich constant (mg g ⁻¹)
n	The heterogeneity factor
K_T	The equilibrium binding constant (L g ⁻¹)
B_T	The Temkin constant (kJ mol ⁻¹)
R^2	Correlation coefficient
R	The universal gas constant (8.314 J mol ⁻¹ K ⁻¹)
T	The absolute temperature (K)
R_L	The dimensionless separation factor
K_1	The pseudo-first-order rate constant (min ⁻¹)
K_2	The pseudo-second-order rate constant (g mg ⁻¹ min ⁻¹)
K_{ip}	The intra-particle diffusion rate constant (mg g ⁻¹ min ^{-0.5})
C	Constant related to the thickness of boundary layer (mg g ⁻¹)
ΔG°	Standard Gibbs free energy change (kJ mol ⁻¹)
ΔH°	Enthalpy change (kJ mol ⁻¹)
ΔS°	Entropy change (kJ mol ⁻¹)

References

- H. Bessbousse, T. Rhallou, J.-F. Verchère and L. Lebrun, Removal of heavy metal ions from aqueous solutions by filtration with a novel complexing membrane containing poly(ethyleneimine) in a poly(vinyl alcohol) matrix, *J. Membr. Sci.*, 2008, **307**, 249–259.
- C. P. Barbosa, G. R. P. Malpass, D. W. Douglas and L. Gomes, Electrochemical Removal of Cu(II) in the Presence of Humic Acid, *J. Braz. Chem. Soc.*, 2010, **4**, 651–658.
- A. da Browksi, Z. Hubicki, P. P. Scielny and E. Robens, Selective removal of the heavy metal ions from waters and industrial wastewaters by ion-exchange method, *Chemosphere*, 2004, **56**, 91–106.
- N. Li and R. Bai, Development of chitosan-based granular adsorbents for enhanced and selective adsorption

- performance in heavy metal removal, *Water Sci. Technol.*, 2006, **54**, 103–113.
- 5 B. E. Reed and S. K. Nonavinakere, Metal Adsorption by Activated Carbon: Effect of Complexing Ligands, Competing Adsorbates, Ionic Strength, and Background Electrolyte, *Sep. Sci. Technol.*, 1992, **27**, 1985–2000.
 - 6 J. E. van Benschoten, B. E. Reed, M. R. Matsumoto and P. J. McGarvey, Metal removal by soil washing for an iron oxide coated sandy soil, *Water Environ. Res.*, 1994, **66**, 168–174.
 - 7 B. Li, F. Su, H.-K. Luo, L. Liang and B. Tan, Hypercrosslinked microporous polymer networks for effective removal of toxic metal ions from water, *Microporous Mesoporous Mater.*, 2011, **138**, 207–214.
 - 8 U. Farooq, J. A. Kozinski, M. A. Khan and M. Athar, Biosorption of heavy metal ions using wheat based biosorbents-a review of the recent literature, *Bioresour. Technol.*, 2010, **101**, 5043–5053.
 - 9 R. Ansari, Application of Polyaniline and its Composites for Adsorption/Recovery of Chromium(vi) from Aqueous Solutions, *Acta Chim. Slov.*, 2006, **53**, 88–94.
 - 10 A. Olad and R. Nabavi, Application of polyaniline for the reduction of toxic Cr(vi) in water, *J. Hazard. Mater.*, 2007, **147**, 845–851.
 - 11 P. A. Kumar, S. Chakraborty and M. Ray, Removal and recovery of chromium from wastewater using short chain polyaniline synthesized on jute fiber, *Chem. Eng. J.*, 2008, **141**, 130–140.
 - 12 L. Ai and J. Jiang, Ultrasonic-assisted synthesis of polyaniline nanosticks, and heavy metal uptake performance, *Mater. Lett.*, 2011, **65**, 1215–1217.
 - 13 L. Seid, D. Chouder, N. Maouche, I. Bakas and N. Barka, Removal of Cd(II) and Co(II) ions from aqueous solutions by polypyrrole particles: Kinetics, equilibrium and thermodynamics, *J. Taiwan Inst. Chem. Eng.*, 2014, **45**, 2969–2974.
 - 14 X. Guo, G. T. Fei, H. Su and L. D. Zhang, High-performance and reproducible polyaniline nanowire/tubes for removal of Cr(vi) in aqueous solution, *J. Phys. Chem. C*, 2011, **115**, 1608–1613.
 - 15 J. Wang, K. Pan, Q. He and B. Cao, Polyacrylonitrile/polypyrrole core/shell nanofiber mat for the removal of hexavalent chromium from aqueous solution, *J. Hazard. Mater.*, 2013, **244–245**, 121–129.
 - 16 H. Wang, J. Ding, B. Lee, X. Wang and T. Lin, Polypyrrole-coated electrospun nanofibre membranes for recovery of Au(III) from aqueous solution, *J. Membr. Sci.*, 2007, **303**, 119–125.
 - 17 N. Jiang, Y. Xu, Y. Dai, W. Luo and L. Dai, Polyaniline nanofibers assembled on alginate microsphere for Cu²⁺ and Pb²⁺ uptake, *J. Hazard. Mater.*, 2012, **215–216**, 17–24.
 - 18 S.-H. Huang and D.-H. Chen, Rapid removal of heavy metal cations and anions from aqueous solutions by an amino-functionalized magnetic nano-adsorbent, *J. Hazard. Mater.*, 2009, **163**, 174–179.
 - 19 C. K. Ahn, D. Park, S. H. Woo and J. M. Park, Removal of cationic heavy metal from aqueous solution by activated carbon impregnated with anionic surfactants, *J. Hazard. Mater.*, 2008, **164**, 1130–1136.
 - 20 R. Coskun and C. Soykan, Preparation of amidoximated polyester fiber and competitive adsorption of some heavy metal ions from aqueous solution onto this fiber, *J. Appl. Polym. Sci.*, 2009, **112**, 1798–1807.
 - 21 D. D. Diogo, M. H. Herbst, R. Ribeiro and V. G. Teixeira, The role of matrix porosity in the adsorption of Cu(II) by amidoxime chelating resins: an electron paramagnetic resonance study, *React. Funct. Polym.*, 2011, **71**, 721–727.
 - 22 B. Gao, Y. Gao and Y. Li, Preparation and chelation adsorption property of composite chelating material poly(amidoxime)/SiO₂ towards heavy metal ions, *Chem. Eng. J.*, 2010, **158**, 542–549.
 - 23 A. F. Shaaban, D. A. Fadel, A. A. Mahmoud, M. A. Elkomy and S. M. Elbahi, Synthesis of a new chelating resin bearing amidoxime group for adsorption of Cu(II), Ni(II) and Pb(II) by batch and fixed-bed column methods, *J. Environ. Chem. Eng.*, 2014, **2**, 632–641.
 - 24 A. Zhang, T. Asakura and G. Uchiyama, The adsorption mechanism of uranium(vi) from seawater on a macroporous fibrous polymeric adsorbent containing amidoxime chelating functional group, *React. Funct. Polym.*, 2003, **57**, 67–76.
 - 25 D. Billaud, E. B. Maarouf and E. Hannecart, Chemical oxidation and polymerization of indole, *Synth. Met.*, 1995, **69**, 571–572.
 - 26 E. B. Maarouf, D. Billaud and E. Hannecart, Electrochemical cycling and electrochromic properties of polyindole, *Mater. Res. Bull.*, 1994, **29**, 637–643.
 - 27 P. S. Abthagir, K. Dhanalakshmi and R. Saraswathi, Thermal studies on polyindole and polycarbazole, *Synth. Met.*, 1998, **93**, 1–7.
 - 28 R. Lazzaroni, A. D. Pryck, C. H. Debraisieux, J. Riga, J. Verbist, J. L. Brédas, J. Delhalle and J. M. André, Electronic structure of conducting polymers from heteroaromatic bicyclic compounds, *Synth. Met.*, 1987, **21**, 189–195.
 - 29 Z. Cai, J. Guo, H. Yang and Y. Xu, Electrochemical properties of electrospun poly(5-cyanoindole) submicron-fibrous electrode for zinc/polymer secondary battery, *J. Power Sources*, 2015, **279**, 114–122.
 - 30 F. A. Cotton, G. Wilkinson, C. A. Murillo and M. Bochmann, *Advanced Inorganic Chemistry*, Wiley-Interscience, New York, 3rd edn, 1995.
 - 31 M. C. Newman and J. T. McCloskey, Predicting Relative Toxicity and Interactions of Divalent Metal Ions: Microtox Bioluminescence Assay, *Environ. Toxicol. Chem.*, 1996, **15**, 275–281.
 - 32 W. Shen, S. Chen, S. Shi, X. Li, X. Zhang, W. Hu and H. Wang, Adsorption of Cu(II) and Pb(II) onto diethylenetriamine-bacterial cellulose, *Carbohydr. Polym.*, 2009, **75**, 110–114.
 - 33 G. Zhang, R. Qu, C. I. Sun, C. Ji, H. Chen, C. Wang and Y. Niu, Adsorption for Metal Ions of Chitosan Coated Cotton Fiber, *J. Appl. Polym. Sci.*, 2008, **110**, 2321–2327.

- 34 C. Duan, N. Zhao, X. Yu, X. Zhang and J. Xu, Chemically modified kapok fiber for fast adsorption of Pb^{2+} , Cd^{2+} , Cu^{2+} from aqueous solution, *Cellulose*, 2013, **20**, 849–860.
- 35 R. Coskun and C. Soykan, Preparation of Amidoximated Polyester Fiber and Competitive Adsorption of Some Heavy Metal Ions from Aqueous Solution onto this Fiber, *J. Appl. Polym. Sci.*, 2009, **112**, 1798–1807.
- 36 P. Zou, Y. Guo and Y. Li, Adsorption of $\text{Pb}(\text{II})$ and $\text{Cd}(\text{II})$ from Contaminated Water by Activated Carbon Fiber, *Environ. Sci. Technol.*, 2012, **35**, 49–53.
- 37 M. Stephen, N. Catherine, M. Brenda, K. Andrew, P. Leslie and G. Corrine, Oxolane-2,5-dione modified electrospun cellulose nanofibers for heavy metals adsorption, *J. Hazard. Mater.*, 2011, **192**, 922–927.
- 38 J. Xiong, C. Jiao, C. Li, D. Zhang, H. Lin and Y. Chen, A versatile amphiprotic cotton fiber for the removal of dyes and metal ions, *Cellulose*, 2014, **21**, 3073–3087.
- 39 S. Wang, L. Wang, W. Kong, J. Ren, C. Liu, K. Wang, R. Sun and D. She, Preparation, characterization of carboxylated bamboo fibers and their adsorption for lead(II) ions in aqueous solution, *Cellulose*, 2013, **20**, 2091–2100.
- 40 Y. Tian, M. Wu, R. Liu, Y. Li, D. Wang, J. Tan, R. Wu and Y. Huang, Electrospun membrane of cellulose acetate for heavy metal ion adsorption in water treatment, *Carbohydr. Polym.*, 2011, **83**, 743–748.
- 41 P. Kampalanonwat and P. Supaphol, Preparation and Adsorption Behavior of Aminated Electrospun Polyacrylonitrile Nanofiber Mats for Heavy Metal Ion Removal, *ACS Appl. Mater. Interfaces*, 2010, **2**, 3619–3627.
- 42 J. C. Igwe, A. A. Abia and C. A. Ibeh, Adsorption kinetics and intraparticulate diffusivities of Hg, As and Pb ions on unmodified and thiolated coconut fiber, *Int. J. Environ. Sci. Technol.*, 2008, **5**, 83–92.
- 43 M. E. Argun, S. Dursun, M. Karatas and M. Guru, Activation of pine cone using Fenton oxidation for $\text{Cd}(\text{II})$ and $\text{Pb}(\text{II})$ removal, *Bioresour. Technol.*, 2009, **99**, 8691–8698.